Hindawi
Advances in Materials Science and Engineering
Volume 2019, Article ID 6027341, 14 pages
https://doi.org/10.1155/2019/6027341

Research Article

Flexural Behavior of the Innovative CA-UHPC Slabs with High and Low Reinforcement Ratios

Yu Feng,[1] **Jianan Qi**,[1] **Jingquan Wang**,[1] **Jiaping Liu**,[2] **and Jianzhong Liu**[2]

[1]*Key Laboratory of Concrete and Prestressed Concrete Structures of Ministry of Education, School of Civil Engineering, Southeast University, Nanjing 211189, China*
[2]*State Key Laboratory of High Performance Civil Engineering Materials, Nanjing 210098, China*

Correspondence should be addressed to Jingquan Wang; wangjingquan@seu.edu.cn

Received 23 January 2019; Accepted 13 March 2019; Published 8 April 2019

Academic Editor: Jose M. Cabrera

Copyright © 2019 Yu Feng et al. This is an open access article distributed under the Creative Commons Attribution License, which permits unrestricted use, distribution, and reproduction in any medium, provided the original work is properly cited.

This paper presents an experimental study on the flexural behavior of an innovative CA-UHPC (ultrahigh-performance concrete containing coarse aggregate) slab with high and low reinforcement ratios. A total of eighteen CA-UHPC slabs were tested to failure under the parameters of longitudinal reinforcement ratio, curing method, and maximum aggregate size. Test results indicated that sufficient longitudinal reinforcement should be embedded to prevent the brittle failure and disastrous damage. High ductile failure mode was observed for specimens with high reinforcement ratio compared with specimens with low reinforcement ratio. Instead of extensively crushing as normal strength concrete, delamination failure appeared in the compression zone of the CA-UHPC slabs owing to the fibers' bridging effect, the yielding of longitudinal reinforcement, and the large expansion of flexural cracks which led to the final failure. The reinforced CA-UHPC slabs demonstrated excellent deformability, and ultimate ratio of deflection to span increased from 1/281 to 1/12 when the reinforcement ratio raised from 0% to 3.45%. Stiffness of the reinforced specimens at the flexural cracking state was about 88% and only approximately 6% at the ultimate state, but nearly 50% of the initial stiffness remained when the longitudinal reinforcements yielded, which indicated superior load resistance ability and excellent postcracking deformability. A new ductility index was proposed to evaluate the postcracking ductility of the CA-UHPC specimens. Finally, test results were compared with the flexural strength predictions of CECS 38-2004, ACI 544.4R, and BS EN 1992.

1. Introduction

UHPC (ultrahigh-performance concrete) is a generic term for a class of advanced cementitious composite materials that reflects excellent strength, stiffness, ductility, and energy dissipation, and these allow more economic and long-life structures than the conventional concrete even without accounting for the increase in structural durability [1–4]. The tensile strength and ultimate tensile strain of UHPC could be as high as 8 MPa and 1% [5–8]. Due to these remarkable mechanical properties, applying of UHPC will decrease self-weight of structures and reduce the cracking risk effectively [9, 10]. Therefore, an increasing number of applications of UHPC in bridges, high-rise buildings, and infrastructure maintenances have been achieved during the past decades [11, 12].

Because of the relatively high compressive strength and ultimate tensile strain of UHPC, which allows for increased strain of the embedded reinforcement and higher stress in the compressive zone, the design concept of UHPC is quite different from the normal strength concrete [13]. To utilize the superior mechanical properties of UHPC adequately, using high-strength steel bars and increasing the reinforcement ratio could be two alternative ways according to the force equilibrium condition [14–16]. Some researchers adopted the first method to achieve material mechanical performance matching. Sumpter et al. [17] compared the structural performance of beams with high-strength reinforcement and conventional reinforcement; test results demonstrated that shear capacity improved distinctly by using high-strength steel reinforcement. Munikrishna et al. [18] studied the shear behavior of RC beams with

high-strength stirrups, and it was found that the required number of high-strength stirrups was less than that of conventional stirrups when the shear capacities were approximately equal. Qi et al. [13] tested eleven UHPC T-beams reinforced with high-strength steel (HSS) bars; results indicated that the HSS-UHPC beam kept nearly 50% of the initial stiffness at ultimate state.

Influences of the reinforcement ratio on UHPC structures have been of great interest also. Yang et al. [19] investigated the flexural behavior of fourteen UHPC beams with six different rebar ratios ranging from 0 to 1.96%; results showed that the ductility improved with the increment of the rebar ratio, but UHPC specimens with a fiber volumetric ratio of 2% exhibited lower ductility compared with the nonfiber ones. Kamal et al. [20] evaluated the flexural behavior of twelve UHPC beams with and without web reinforcement; the promotion impact of reinforcement ratio on structural ductility was also confirmed. Kahanji et al. [21] conducted flexural test of eight UHPC beams with and without reinforcement rebar, and it was found that flexural moment capacity and stiffness increased with the fiber volume fraction. Flexural behaviors of four UHPC beams with different reinforcement ratios (0%~1.71%) were experimentally and numerically investigated by Yoo et al. [22] also, and test results indicated that the postcracking stiffness and load carrying capacity increased with the reinforcement ratio, whereas the first cracking load decreased. Hasgul et al. [23] studied the flexural behavior of eight UHPC beams with low and high reinforcement ratios (0.9%, 1.9%, 2.8%, and 4.3%), and results demonstrated that the ductile flexural behavior could be achieved even at high reinforcement ratios because of its high compressive strength and deformation capacity.

Although there are some research achievements about the influences of reinforcement ratio on structural performance of UHPC beams, most of the research studies concentrate on the low reinforcement ratio [24, 25]. As far as the authors are aware, less research existed on UHPC slabs with high reinforcement ratio and inadequacy of data samples may reduce the scope of the conclusions; comprehensive understanding is needed to obtain better structural performance and broaden the application of UHPC slabs in civil engineering.

This paper mainly aims at the flexural behavior of the innovative CA-UHPC slabs with high and low longitudinal reinforcement ratio via an experimental program on eighteen CA-UHPC slabs. The effects of longitudinal reinforcement ratio, curing method, and maximum aggregate size are investigated, including failure mode, postcracking performance, ductility, and stiffness degradation of the CA-UHPC specimens. In addition, the applicability of CECS 38-2004, ACI 544.4R, and BS-EN 1992 is compared to evaluate flexural capacity of the innovative CA-UHPC slabs with high and low reinforcement ratios.

2. Experimental Program

2.1. Specimen Dimensions. A total of eighteen specimens were designed to research the bending performance of the innovative CA-UHPC slabs, and all the specimens were manufactured in pairs to control the discreteness of data (Table 1). Due to the different reinforcement ratios of 0%, 1.41%, and 3.45%, test specimens are classified into Series R0, Series R1.13, and Series R3.45. All the slab specimens have the same external physical dimension of 1500 mm × 350 mm × 160 mm. Geometry dimensions and reinforcement diagram of the test specimens are shown in Figure 1.

2.2. Mix Properties and Specimen Preparation

2.2.1. Raw Materials. The innovative CA-UHPC (ultrahigh-performance concrete containing coarse aggregate) which is budget saving and shrinkage inhabiting [26, 27] has been developed in this experimental program. Two kinds of clean medium coarse sands with the fineness modulus of 3.1 and 2.8 are adopted in the innovative UHPC system, which is obviously different from the UHPC material in general sense. The aggregates consisting of basalt and limestone are offered by four different domestic manufacturers, particle size of them ranges from 5 mm to 8 mm. Weight content of the main components of the innovative UHPC material is all illustrated in Figure 2, and the water-binder ratio (W/B) of the innovative CA-UHPC is 0.16.

High-strength straight steel fiber coated with a thin layer of copper is mixed in the matrix with the volume fraction of 2% to improve the tensile strength and ductility of UHPC matrix. Length and diameter of the steel fiber are 13 mm and 0.2 mm, respectively, and the yielding strength is 2900 MPa.

2.2.2. Site Casting and Curing Regime. High-quality wood formworks are adopted for the site pouring of the specimens, as shown in Figure 3. Field mixing of the innovative CA-UHPC was conducted by the shaft mixer which provided 0.3 m^3 concrete once, and the mixing processes are as follows. Cementitious materials and aggregates need to be dry-mixed for one minute first, and then water and additives were added to stir for four minutes. The high-strength steel fiber was put in terminally and continued stirring for three minutes. Matrix of the CA-UHPC were poured out for the forming of specimens after mixing evenly, and this operation should run parallel to the casting of samples for material properties test.

Curing regime of the experiment consists of the natural curing and steam curing method. For the natural curing, test specimens need to be demolded immediately after casting for 24 h and maintained in the standard curing room at the temperature of 20 ± 2°C. The relative humidity needs to be no less than 95%, and the surface of the specimens should keep wet and not be flushed directly by water, as suggested by the Chinese code of test method for mechanical properties of ordinary concrete (GB/T 50081-2002). For the steam curing, heat maintenance starts after 24 h of casting also. Firstly, heating the curing box (Figure 3) to 90°C in a rate of 10°C/h and keeping the temperature (90 ± 2°C) for 48 h, and then cooling down at the same rate until the difference between temperature of specimen surface and ambient temperature is no more than 20°C.

Table 1: Main parameters of the CA-UHPC slab specimens.

Specimen ID		a (mm)	b (mm)	d (mm)	h (mm)	l_s (mm)	l (mm)	ρ_s (%)	Mix type
Series R0	R0-S-8	400	350	/	160	1300	1500	0	A
	R0-S-5	400	350	/	160	1300	1500	0	B
	R0-N-8	400	350	/	160	1300	1500	0	C
Series R1.13	R1.13-S-8	400	350	114	160	1300	1500	1.13	A
	R1.13-S-5	400	350	114	160	1300	1500	1.13	B
	R1.13-N-8	400	350	114	160	1300	1500	1.13	C
Series R3.45	R3.45-S-8	400	350	130	160	1300	1500	3.45	A
	R3.45-S-5	400	350	130	160	1300	1500	3.45	B
	R3.45-N-8	400	350	130	160	1300	1500	3.45	C

S = steam curing; N = natural curing; 5/8 = 5 mm/8 mm aggregate size; a = length of pure bending zone; b = width of the web; d = effective depth; h = slab height; l_s = span of the slab; l = length of the slab; ρ_s = longitudinal reinforcement ratio. Two specimens were precast in each ID, and subsequent researches are aimed at the average value of the two specimens.

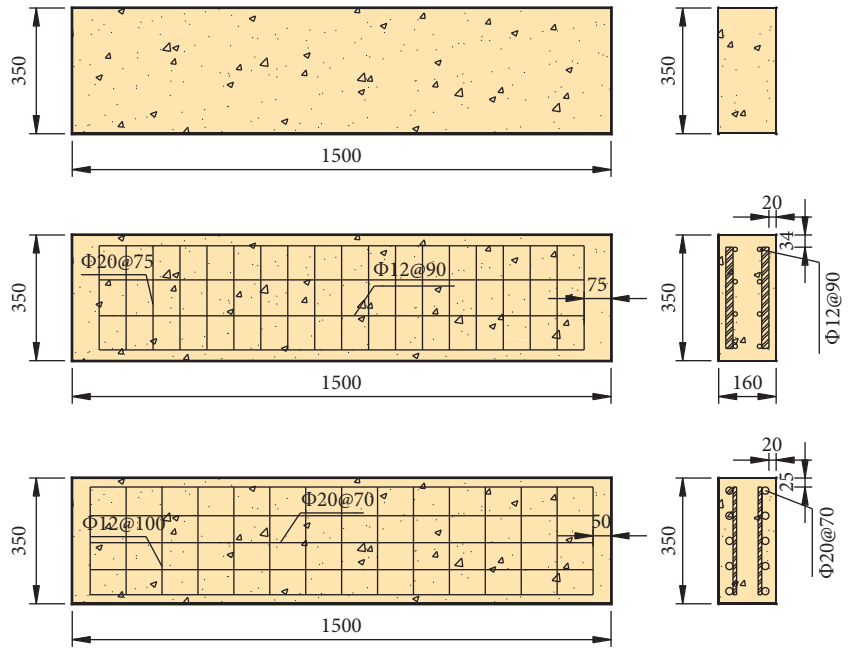

Figure 1: Dimensions and reinforcement diagram of test specimens. (a) R0-S/N-8/5. (b) R1.13-S/N-8/5. (c) R3.45-S/N-8/5.

2.3. Material Properties. According to the Chinese code of reactive powder concrete (GB/T 31387-2015), all the specimens for material property experiment were tested after 28 d curing age, in which, three groups of cube specimens with dimensions of 100 mm × 100 mm × 100 mm were prepared for the compressive strength test, while six prism specimens with dimensions of 100 mm × 100 mm × 300 mm were utilized to determine the elastic modulus and Poisson ratio. The test method of bending toughness and initial cracking strength are based on the Chinese technical specification for fiber reinforced concrete structures (CECS 38-2004), and prism specimens with the size of 100 mm × 100 mm × 400 mm were utilized after maintenance for 28 d. Material properties of the innovative CA-UHPC are summarized in Table 2.

Longitudinal and transverse reinforcement of the slab specimens consists of two types of steel bars with the diameter of 20 mm and 12 mm, while the yielding strength is 350.5 MPa and 446.6 MPa, respectively. In particular, layout of the reinforcement in slabs of Series R1.13 and Series R3.45 is reserved. It should be noted that no stirrups and bend-up bars were set in all the specimens. Material properties of reinforcement bars are presented in Table 3.

2.4. Test Setup and Loading Mechanism. As shown in Figure 4, static performance tests of the slabs are conducted through the four-point bending experiments. Simply supported boundary condition is applied, span of the slabs is 1300 mm, and length of the pure bending zone is 400 mm. Electrohydraulic servo actuator with the maximal measuring range of 1000 kN is chosen to apply the monotonic load, while extra force sensor is installed to ensure the accuracy of load data. Three groups of LVDT are set on midspan and bearings to monitor the displacement of specimens during each load stage, and strain gauges are arranged at the middle of the bottom of longitudinal reinforcements uniformly.

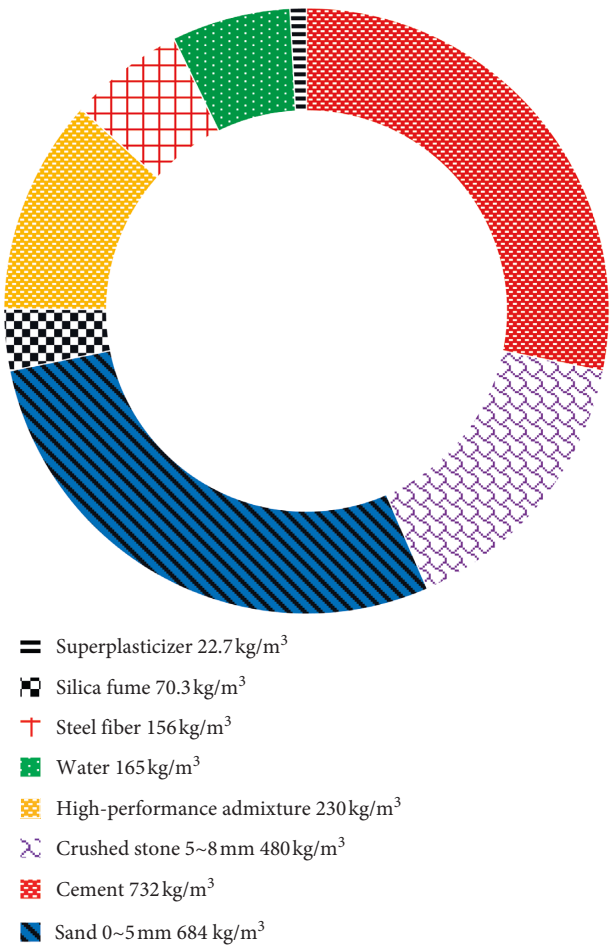

Figure 2: Weight per cubic meter of components of the innovative CA-UHPC material.

In order to inspect the loading system and eliminate inelastic deformation, all the slabs were loaded and unloaded repeatedly according to 40% of the predicted cracking load before officially loading. Preloading will not stop until deformation and strain are kept stable approximately, and the specific test processes are as follows. Firstly, loading to 80% of the predicted cracking load in the speed of 10~20 kN per step and recording the deflection and strain. Then, reducing the load step to find out the actual cracking load of the specimen cautiously; displacement control is recommended once visible cracks are found. Finally, unloading the actuator slowly when the ultimate load is reached, and the cracks are too large for the sake of safety.

3. Experimental Results and Discussions

3.1. Failure Mode and Crack Distribution. All the eighteen CA-UHPC slabs were tested to failure. For the reinforced specimens in Series R1.13 and Series R3.45, bending cracks first appeared at the bottom near the midspan where the largest tensile force has been withstood. Because of the absence of shear reinforcement and relatively high longitudinal reinforcement ratio, width of diagonal cracks was even slightly larger than that of bending cracks in the early loading process. With the increment of applied load, flexural cracks developed rapidly at decreasing of the fiber bridging effect with intensive sizzle sound especially when approaching the ultimate bearing capacity (nearly 200 kN for Series R1.13 and 500 kN for Series R3.45); the yielding of longitudinal reinforcement and the large expansion of flexural cracks led to the final failure. In general, ductile flexural failure occurred in all the reinforced CA-UHPC slabs, and typical failure mode and crack distribution of the specimens with high reinforcement ratio at failure are shown in Figure 5. Different from conventional RC structures, it was interesting to find that extensively concrete crushing was not observed even when exceeding the ultimate compressive strain of UHPC. Delamination failure appeared in compression zone of the CA-UHPC slabs owing to the fibers bridging effect. As steel fibers bridging the adjacent concrete layers and keeping connected, the surface layer of the CA-UHPC specimens warped instead of crushing, which presented the multilayer bridged by interlaminar fibers failure mode that the steel fiber remained even though the concrete layer was separated.

For the plain CA-UHPC slabs in Series R0, flexural cracks appeared first in the pure bending area closed to the midspan. As the applied load increased, the cracks developed rapidly and associated with the sound of fibers pulling out, and some main flexural cracks formed quickly due to the decreasing of fiber bridging effect and directly caused the final failure when approaching to ultimate bearing capacity (nearly 100 kN). Therefore, sufficient longitudinal reinforcement should be embedded to prevent the brittle failure and disastrous damage that is unexpected.

Table 4 summarizes important characteristic information of all the specimens. As initial cracking strength is primarily dominated by the tensile strength of UHPC matrix, nominal stress at initial cracking in different series is basically consistent. This characteristic also indicated that CA-UHPC could still ensure excellent and stable material properties even cast in place and is suitable for large-scale construction on-site. Applied load corresponding to different crack widths increases significantly with the increment of the reinforcement ratio, while the same trend appears on the deflection which reflects the enhancement of ductility.

3.2. Structural Behavior

3.2.1. Load versus Midspan Deflection. Figure 6 presents the relationship between load and midspan deflection of all the specimens. A similar pattern is reflected that the load-deflection curves and displays linear relationship before bending cracks occur and almost keep linear after flexural cracking with a slightly decline in stiffness, but the stiffness of specimens drops when the longitudinal reinforcement yields. As shown in the deflection curve, ductility of specimens increases with the increment of the reinforcement ratio obviously. It should be noted that a long ductile plateau stage is detected for specimens with high reinforcement ratio (Series R3.45).

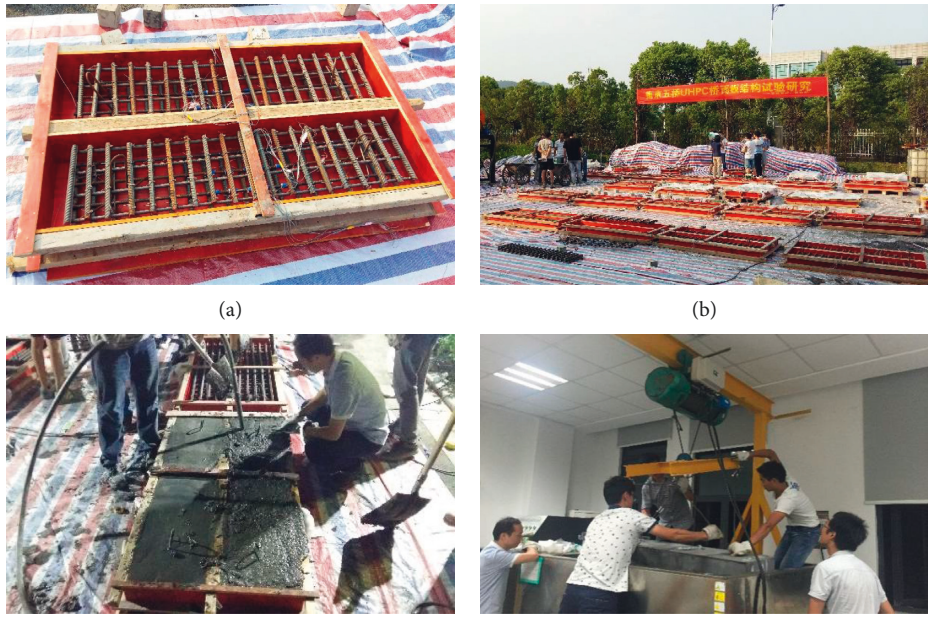

(a) (b) (c) (d)

Figure 3: Pouring and curing process of the innovative CA-UHPC. (a) Formwork. (b) Site casting. (c) Vibration. (d) Stream curing.

Table 2: Material properties of CA-UHPC.

Mix type	Curing method	Aggregate size (mm)	E_c (GPa)	ν	f_{cu} (MPa)	f_{MOR} (MPa)	$f^{\dagger}_{MOR}$ (MPa)	G_f (kJ·m^{-2})
A	Steam curing	8	50.4	0.20	165.7	13.59	19.91	24.58
B	Steam curing	5	49.5	0.20	168.5	13.92	20.16	21.52
C	Natural curing	8	49.3	0.21	146.7	12.66	17.13	24.11

E_c = elasticity modulus; ν = Poisson's ratio; f_{cu} = cubic compressive strength; f_{MOR} = flexural strength at cracking state; $f^{\dagger}_{MOR}$ = flexural strength at ultimate state; G_f = fracture energy.

Table 3: Material properties of reinforcement bars in Series R3.45.

Steel type	d_s (mm)	A_s (mm^2)	F_y (kN)	f_y (MPa)	F_u (kN)	f_u (MPa)	E_s (GPa)
Longitudinal reinforcement	20	314.2	110.1	350.5	183.0	582.5	200
Transverse reinforcement	12	113.1	50.5	446.6	64.1	566.3	200

Reinforcement layout of specimens in series R1.13 is contrary to that in series R3.45, which means diameter of the longitudinal reinforcement in series R1.13 is 12 mm and diameter of the transverse reinforcement is 20 mm.

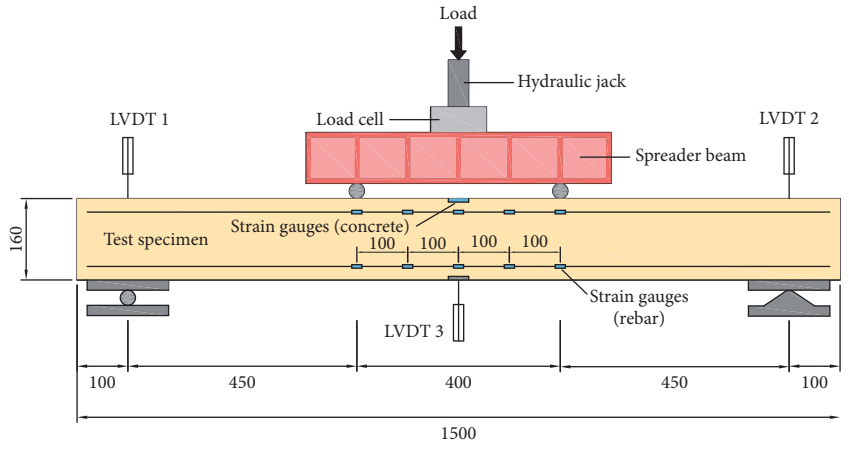

Figure 4: Loading mechanical scheme.

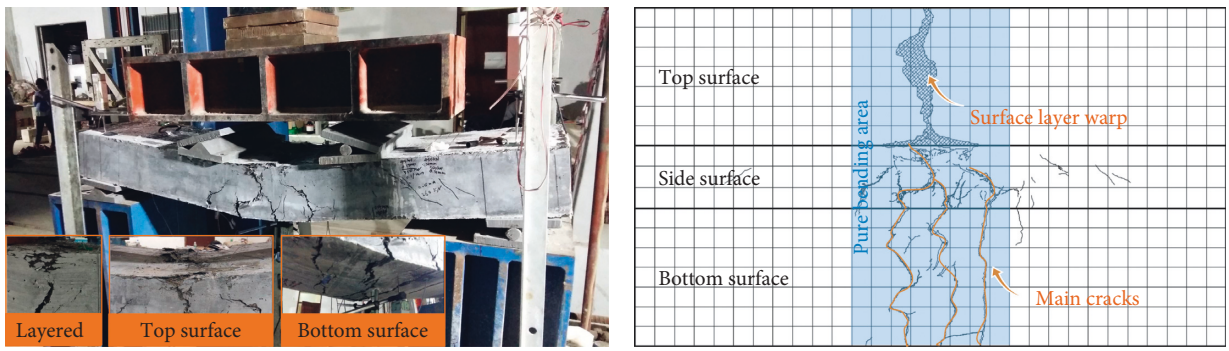

(a) (b)

Figure 5: (a) Typical failure mode and (b) typical crack distribution of the slabs in Series R3.45.

3.2.2. Load versus Longitudinal Reinforcement Strain. Strain gauges evenly arranged at the midspan section of the longitudinal reinforcement are adopted to monitor the change of steel strain, and relationship curves of load versus longitudinal reinforcement strain of all the specimens are shown in Figure 7. Stresses in the tension side of longitudinal reinforcement stay at low level before cracking, and the curves are approximately kept linear; growth rate of the steel stress accelerates dramatically after flexural cracking until yielding strength. After entering the yielding state, strains of the longitudinal reinforcement continue to rise quickly for the increment of deflection until failure. As ductile failure still occurs on the innovative CA-UHPC slabs with high reinforcement ratio, steel bars with high strength and ductility would be recommended for the CA-UHPC structures.

3.2.3. Load versus Top and Bottom Concrete Surface Strain of Midspan Section. Figure 8 depicts relationship between the concrete strain of midspan section and the applied load of the test CA-UHPC slabs, in which positive value represents the tensile strain while negative value represents the compressive strain. As seen in these figures, compressive strain of concrete increases slowly before cracking and acts as linear behavior and the rapid growth of the concrete compressive strains begins to appear right after cracking and keep expanding until failure. The concrete strain of tension and compression side of the slabs nearly maintains symmetry before flexural cracks occur. For the plain CA-UHPC slabs in Series 0, it should be noted that the cracking tensile strain is larger than 200 μ which reflects excellent material properties. While for the reinforced CA-UHPC slabs, extensively concrete crush is not observed even when ultimate compressive strain of UHPC (≈3,500 μ) is exceeded, which is quite different from the failure mode of normal strength concrete.

3.3. Effects of Curing Method and Aggregate Size. Thermal treatments of traditional UHPC are mainly preferred in order to reduce curing time and increase mechanical strengths [28–30], and it does not usually contain coarse aggregates larger than 6-7 mm in size [21]. It is difficult to meet the curing condition during large-scale on-site construction. However, the addition of coarse aggregate can save budget and broaden the application field of UHPC by reducing the amount of glue material and decreasing hydration temperature rise. Therefore, effects of the curing method and maximum aggregate size are studied in this paper also. As shown in Figure 9, results indicate that flexural strength increases approximately linearly with the increment of longitudinal reinforcement ratio, while maximum aggregate size and curing method have no significant influences on structural behavior of the innovative CA-UHPC slabs.

3.4. Effects of Reinforcement Ratio on Deflection Ductility. The ductility index is always utilized to characterize the ductility of reinforced concrete specimens, and the deflection ductility index is always adopted for the simplicity of its expressions. These expressions [31] are usually used as ductility index:

$$\mu_p = \frac{\Delta_p}{\Delta_y}, \qquad \mu_u = \frac{\Delta_u}{\Delta_y}, \tag{1}$$

where Δ_p is the midspan deflection at peak load, Δ_y is the midspan deflection at the longitudinal reinforcement yielding, and Δ_u is the midspan deflection at ultimate load which is geometrically determined by the point corresponding to 80% of the maximum load [32]. Qi et al. [33] put forward a new ductility index, which is expressed in the form of dividing ultimate deflection by flexural cracking deflection to characterize the postcracking ductility capacity:

$$\mu_{cr} = \frac{\Delta_u}{\Delta_{cr}}. \tag{2}$$

The ductility indices of the UHPC slabs are summarized in Table 5. It can be seen from the results that longitudinal reinforcement shows significant influences on the postcracking capacity. Postcracking ductility of the innovative CA-UHPC slabs increases as the reinforcement ratio increases obviously and gradually decreased with the expansion of cracks, while the ductility index μ_p decreases as the

Table 4: Summary of experimental data.

Specimen ID	First cracking			Crack width of 0.05 mm		Crack width of 0.10 mm		Crack width of 0.15 mm		Reinforcement yielding state		Peak load		Ultimate load		Failure mode
	P_{cr} (kN)	Δ_{cr} (mm)	σ_{cr} (MPa)	$P_{0.05}$ (kN)	$\Delta_{0.05}$ (mm)	$P_{0.10}$ (kN)	$\Delta_{0.10}$ (mm)	$P_{0.15}$ (kN)	$\Delta_{0.15}$ (mm)	P_y (kN)	Δ_y (mm)	P_{max} (kN)	Δ_{max} (mm)	P_u (kN)	Δ_u (mm)	
R0-S-8	94.66	1.63	14.3	98.83	1.78	100.22	2.02	105.1	2.74	Unreinforced		105.1	2.735	84.22	4.62	Flexural[‡]
R0-S-5	96.05	1.5	14.5	100.92	1.75	107.53	2.07	110.66	2.20	Unreinforced		115.88	2.82	92.57	4.51	Flexural[‡]
R0-N-8	79.34	1.69	12.0	81.08	1.71	100.2	2.94	105.1	3.8	Unreinforced		107.53	4.56	86.3	6.02	Flexural[‡]
R1.13-S-8	76.91	2.17	11.6	83.87	2.61	100.57	3.56	123.19	4.81	176.44	9.35	200.1	20.2	160.08	48.42	Flexural[†‡]
R1.13-S-5	75.86	1.88	11.4	80.39	2.13	110.32	2.73	151.03	4.62	169.13	5.49	214.72	17.75	178.87	46.85	Flexural[†‡]
R1.13-N-8	77.26	1.64	11.6	80.04	1.72	104.4	2.68	150.34	4.86	176.09	6.69	194.53	16.38	155.56	41.03	Flexural[†‡]
R3.45-S-8	82.48	1.43	12.4	88.39	1.49	199.75	3.31	258.56	4.28	455.53	8.96	486.5	15.66	389.2	107.2	Flexural[†‡]
R3.45-S-5	80.39	1.71	12.1	83.52	1.73	171.22	3.45	273.88	5.45	459.01	12.88	464.58	16.56	371.66	99.91	Flexural[†‡]
R3.45-N-8	82.13	1.05	12.4	84.91	1.11	175.04	2.69	325.38	5.4	430.82	9.09	479.2	17.83	383.36	84.5	Flexural[†‡]

P_{cr} = flexural cracking load; Δ_{cr} = flexural cracking deflection; σ_{cr} = nominal stress at initial cracking; P_y = longitudinal reinforcement yielding load; Δ_y = longitudinal reinforcement yielding deflection; P_{max} = peak load; Δ_{max} = peak load deflection; P_u = ultimate load; Δ_u = ultimate load deflection; [†]yielding of longitudinal reinforcement; [‡]large expansion of flexural crack.

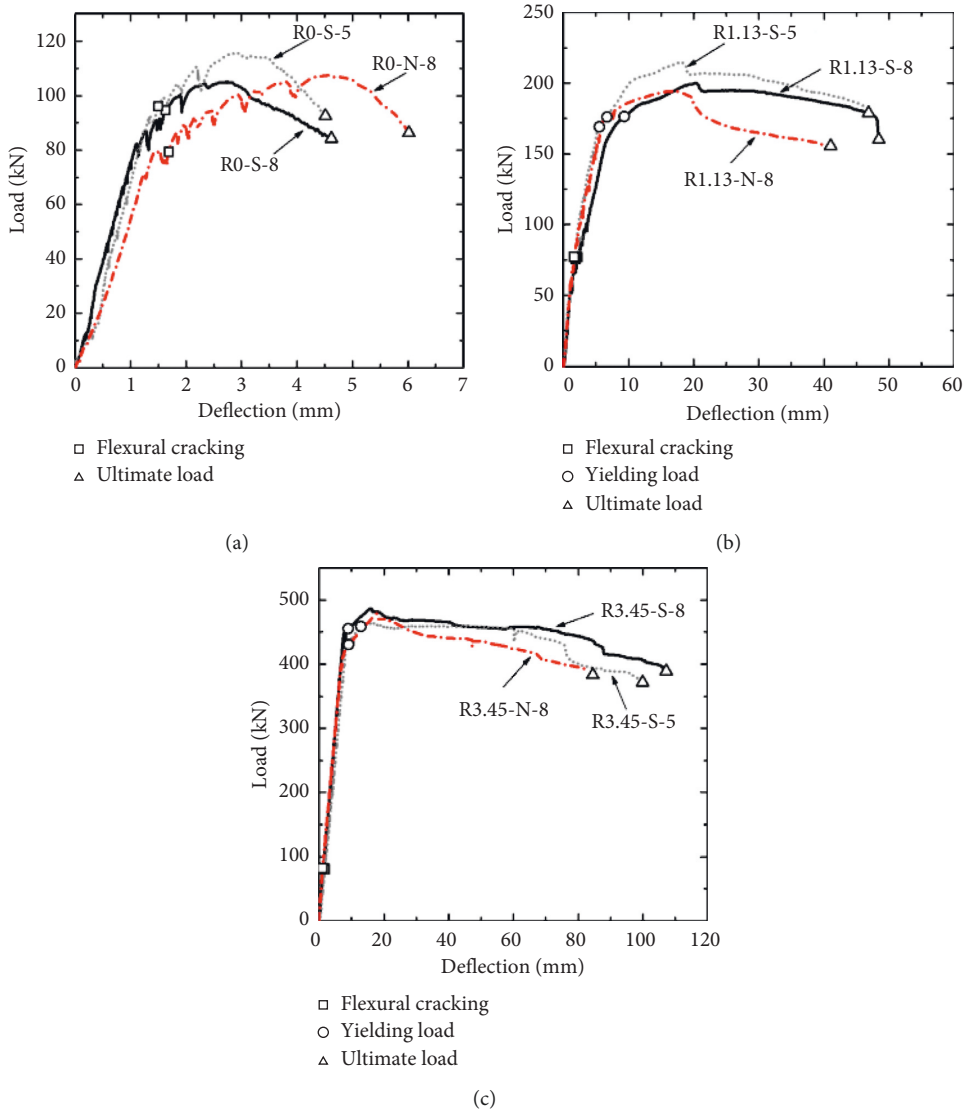

Figure 6: Load versus midspan deflection.

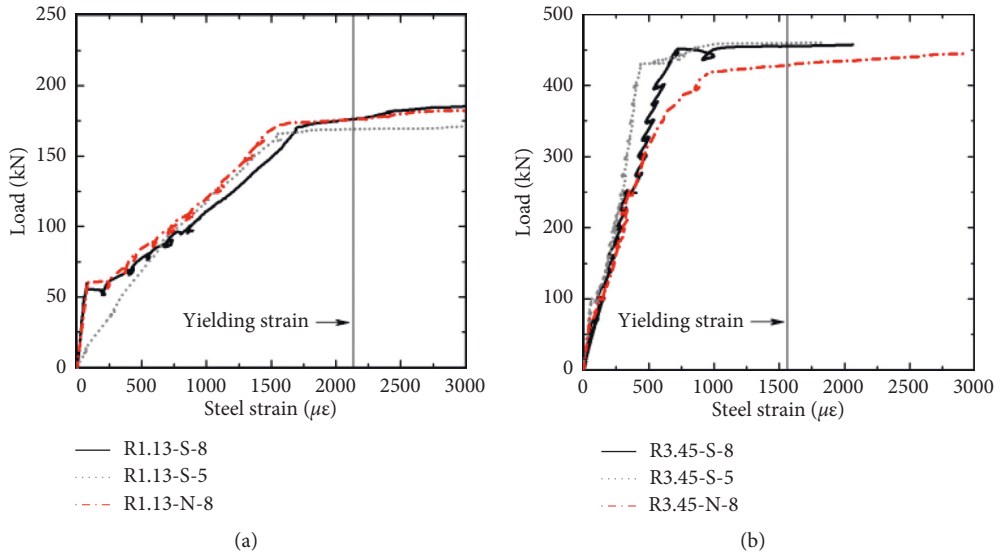

Figure 7: Load versus longitudinal reinforcement strain.

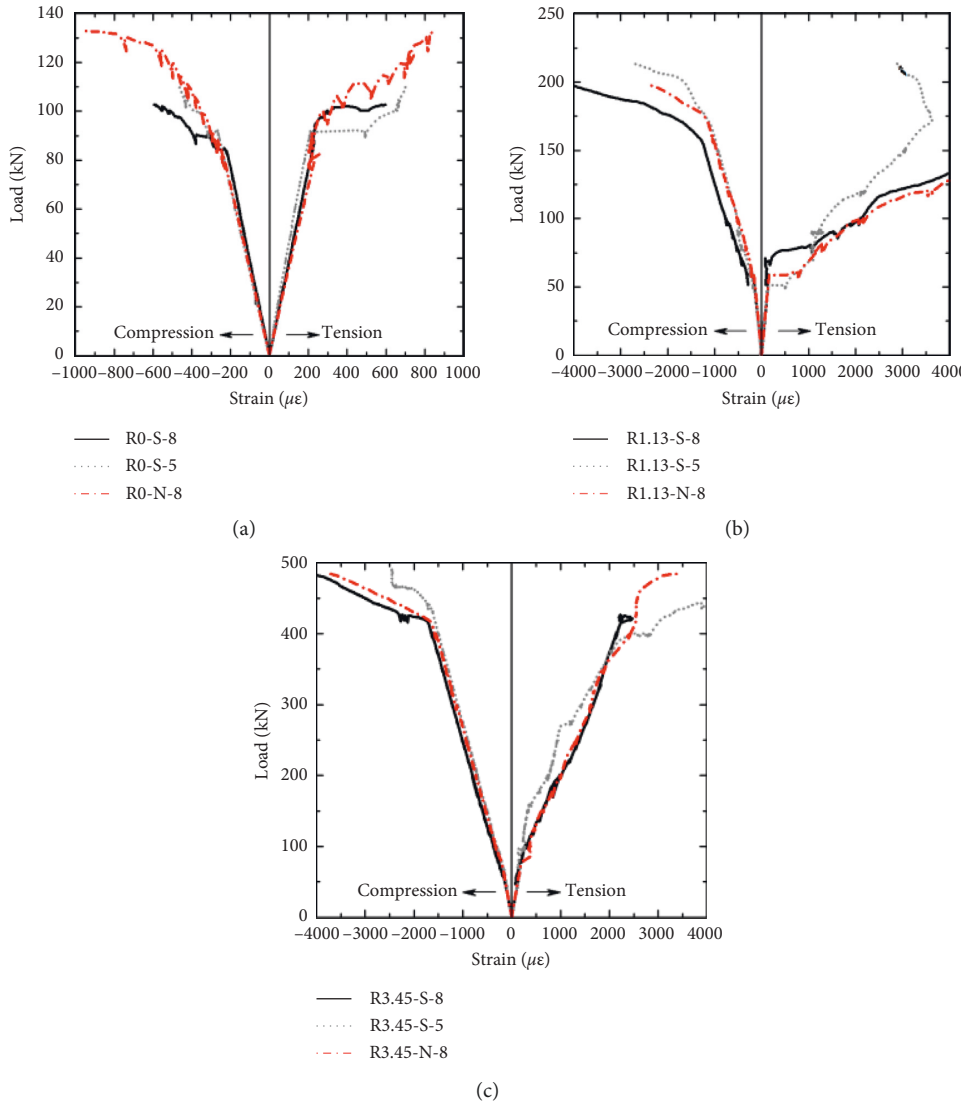

Figure 8: Load versus top and bottom concrete surface strains of midspan section.

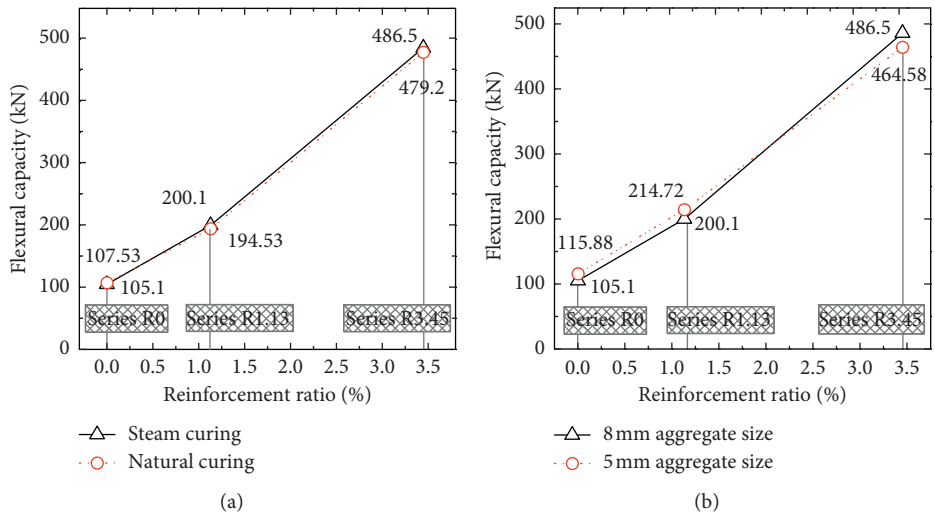

Figure 9: Effects of curing method and aggregate size on flexural capacity.

Table 5: Postcracking capacity and deformability analysis.

Specimen ID	Postcracking capacity				Deflection ductility					
	P_u/P_{cr}	$P_u/P_{0.05}$	$P_u/P_{0.10}$	$P_u/P_{0.15}$	$\Delta_{0.05}/\Delta_{cr}$	$\Delta_{0.10}/\Delta_{cr}$	$\Delta_{0.15}/\Delta_{cr}$	Δ_p/Δ_y	Δ_u/Δ_y	Δ_u/Δ_{cr}
R0-S-8	0.89	0.85	0.84	0.80	1.09	1.24	1.68	/	/	2.83
R0-S-5	0.96	0.92	0.86	0.84	1.17	1.38	1.47	/	/	3.01
R0-N-8	1.09	1.06	0.86	0.82	1.01	1.74	2.25	/	/	3.56
R1.13-S-8	2.08	1.91	1.59	1.30	1.20	1.64	2.22	2.16	5.18	22.31
R1.13-S-5	2.36	2.23	1.62	1.18	1.13	1.45	2.46	3.23	8.53	24.92
R1.13-N-8	2.01	1.94	1.49	1.03	1.05	1.63	2.96	2.45	6.13	25.02
R3.45-S-8	4.72	4.40	1.95	1.51	1.04	2.31	2.99	1.75	11.96	74.97
R3.45-S-5	4.62	4.45	2.17	1.36	1.01	2.02	3.19	1.29	7.76	58.43
R3.45-N-8	4.67	4.51	2.19	1.18	1.06	2.56	5.14	1.96	9.30	80.48

reinforcement ratio increases which in accordance with the researches of Yoo and Yoon [34]. The proposed new ductility index excellently reflects the effects of reinforcement ratio on deflection ductility, and μ_{cr} of specimens with the reinforcement ratios of 0%, 1.13%, and 3.45% was 2.83, 22.31, and 74.97, respectively. The ultimate ratio of deflection to span increases from 1/281 to 1/12 when the longitudinal reinforcement ratio of the innovative CA-UHPC slabs ranges from 0% to 3.45%.

3.5. Effects of Reinforcement Ratio on Specimen Stiffness. In order to clarify the law of stiffness degradation of the CA-UHPC specimens, the relationship between the specimen stiffness and the ratio of the midspan deflection Δ at any time divided by the midspan deflection Δ_{cr} corresponding to flexural cracking load is presented in Figure 10; the secant stiffness is adopted here. As can be seen in the figure, the longitudinal reinforcement ratio presents great influences on stiffness of the specimens. Stiffness of the plain slabs (Series R0) descends rapidly and continuously until failure due to the absence of longitudinal reinforcement. However, the rate of stiffness degradation of the reinforced slabs (Series R1.13 and R3.45) apparently slows down after the longitudinal reinforcement yielding, although the trend of the curve is the same.

Structural performances of the innovative CA-UHPC slabs evaluated by the stiffness degradation in different states are summarized in Table 6. The parameters k_0, k_{cr}, k_y, and k_u represent the stiffness at initial state, flexural cracking state, steel bar yielding state, and ultimate state, respectively. There is no significant decline on the stiffness at initial cracking except for specimen R0-S-8 (71%) and specimen R1.13-S-8 (72%); nearly half the initial stiffness still remains when the longitudinal reinforcement is yielding. Therefore, reinforcement with high strength and long yield platform would be appropriate choice for the CA-UHPC structures. At the ultimate state, only approximately 6% of the initial beam stiffness remained.

4. Comparison between Current Flexural Provisions

According to the experimental data, three current concrete codes, including Chinese Code (CECS 38-2004), American Code (ACI 544.4R) and British Standard (BS EN 1992), are selected to predict the flexural bearing capacity of test specimens. In the CECS 38-2004 model, the equivalent stress blocks for the compressive and tensile regions of the concrete are used to calculate the beam moment capacities, and maximum strain value in the outermost compression fiber of concrete is basically assumed as 0.003, as shown in Figure 11. Bending capacity of normal section of rectangular section flexural members can be calculated by the following equations:

$$M_{fu} = f_{fc} bx\left(h_0 - \frac{x}{2}\right) + f'_y A'_s (h_0 - a'_s) - f_{ftu} bx_t \left(\frac{x_t}{2} - a\right),$$

$$f_{fc} bx = f_y A_s - f'_y A'_s + f_{ftu} bx_t,$$

$$f_{ftu} = f_t \beta_{tu} \lambda_f, \tag{3}$$

where f_{fc} denotes the design value of axial compressive strength of UHPC, while f_{ftu} is the tensile strength of equivalent rectangular stress of the UHPC in tension zone, λ_f is the characteristic value of steel fiber content, and β_{tu} is fiber tensile influence coefficient, they can be calculated by the CECS Code. Additionally, h_0 is the effective depth, b is cross-sectional width, x and x_t are depth of equivalent compressive and tensile stress block, respectively.

Relative error of the prediction value calculated by different codes is summarized in Table 7, and the results indicate that the Chinese Code presents the minimum prediction error. Prediction accuracy of the ACI 544.4R for specimens in Series R1.13 is better than that of Series R3.45, which illustrates that it may not suitable for the flexural calculation of CA-UHPC specimens with high reinforcement ratio. British Standard may be the worst calculation method for the innovative CA-UHPC slabs, and the average error even reaches nearly 60%. As the innovative CA-UHPC has excellent material properties, contribution of the concrete tensile strength should be considered when carrying out the prediction of bending capacity. If combined with the calculation method of concrete tensile zone proposed by CECS 38-2004, the average relative error of Britain Standard will drop to 0.19. In general, evaluation of all the three existing codes on flexural capacity of the innovative CA-UHPC slabs are

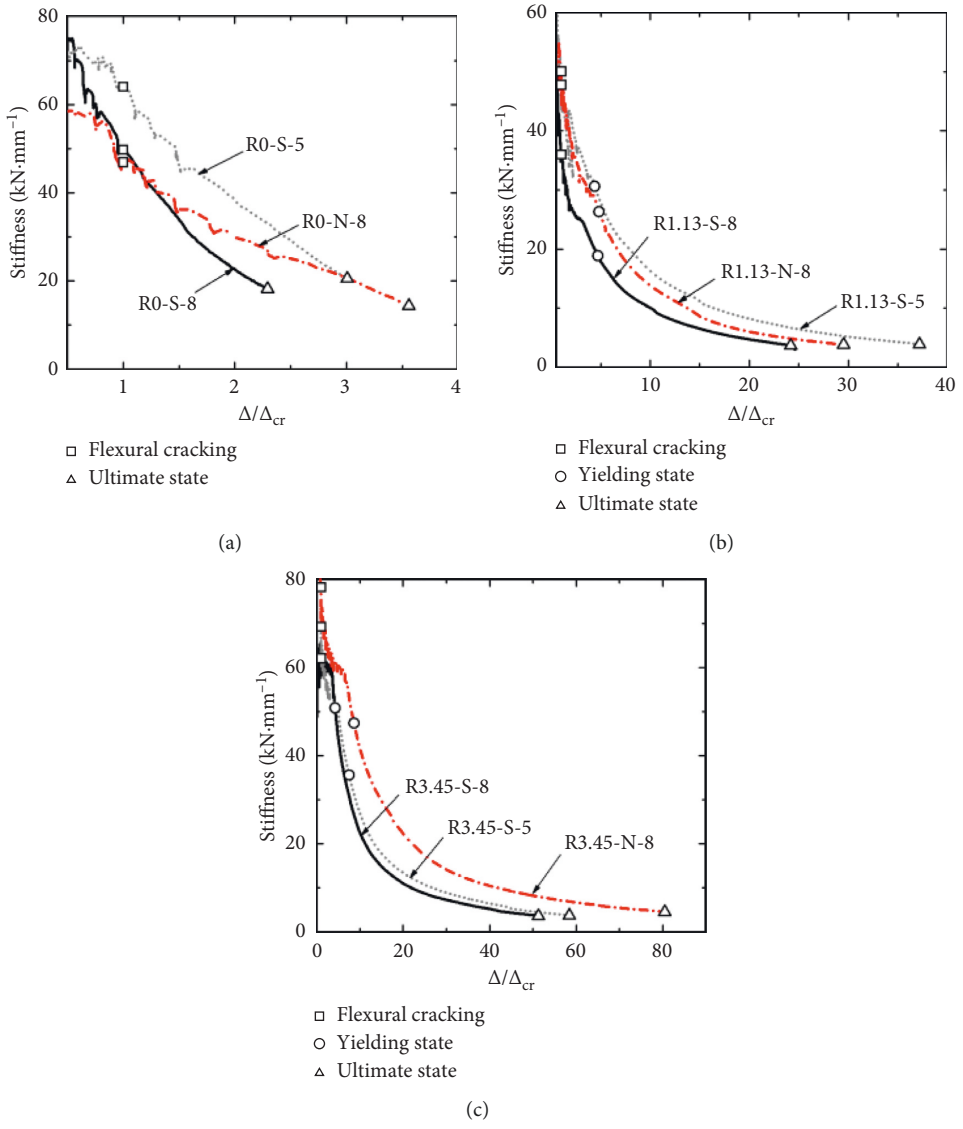

Figure 10: Stiffness degradation analysis.

Table 6: Relative stiffness degradation.

Specimen ID	Flexural cracking		Yielding state		Ultimate state	
	Δ_{cr}/Δ_u	k_{cr}/k_0	Δ_y/Δ_u	k_y/k_0	Δ_u/Δ_u	k_u/k_0
R0-S-8	0.44	0.71	/	/	1.00	0.26
R0-S-5	0.33	0.91	/	/	1.00	0.32
R0-N-8	0.28	0.79	/	/	1.00	0.24
R1.13-S-8	0.04	0.72	0.19	0.37	1.00	0.07
R1.13-S-5	0.03	0.80	0.12	0.51	1.00	0.06
R1.13-N-8	0.03	0.93	0.16	0.49	1.00	0.07
R3.45-S-8	0.02	0.90	0.08	0.73	1.00	0.05
R3.45-S-5	0.02	0.97	0.13	0.50	1.00	0.05
R3.45-N-8	0.01	0.98	0.11	0.59	1.00	0.06

conservative, and the prediction of the Chinese CECS 38-2004 code has relatively the best accuracy with a relative error of 0.16.

5. Conclusions

Eighteen innovative CA-UHPC specimens with high and low reinforcement ratios were tested to failure, and the effects of the longitudinal reinforcement ratio, curing method, and aggregate size on the flexural behavior of the innovative CA-UHPC slabs were investigated. The deflection ductility, flexural stiffness degradation, and post-cracking behaviors of the test specimens were discussed. In addition, three different current calculation specifications for bending resistance were compared to evaluate the flexural capacity of the innovative CA-UHPC slabs. Based on the experimental observations and results, the following conclusions can be drawn:

(1) Sufficient longitudinal reinforcement should be provided in the innovative CA-UHPC slabs, and ductile failure occurred even with high reinforcement ratio. Instead of extensively crushing in

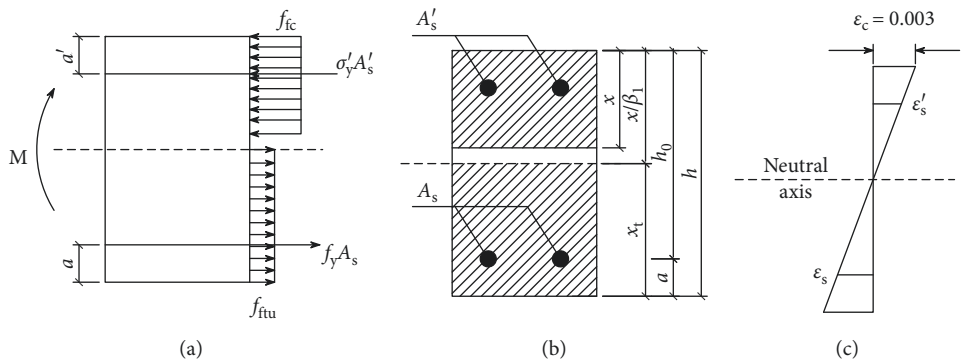

Figure 11: Stress-strain distribution for reinforced UHPC beams in CECS 38-2004.

Table 7: Calculation result comparison of different codes.

Specimen ID		EV	CECS 38-2004		ACI 544.4R		BS EN 1992		BS EN 1992*	
			CV	RE	CV	RE	CV	RE	CV	RE
Series R1.13	R1.13-S-8	200.1	172.57	0.14	245.29	0.23	64.96	0.68	268.22	0.34
	R1.13-S-5	214.72	173.45	0.19	247.99	0.15	64.97	0.70	270.24	0.26
	R1.13-N-8	194.53	166.43	0.14	226.97	0.17	64.92	0.67	254.01	0.31
Series R3.45	R3.45-S-8	486.5	399.53	0.18	309.15	0.36	237.35	0.51	439	0.10
	R3.45-S-5	464.58	400.8	0.14	309.97	0.33	237.44	0.49	441.26	0.05
	R3.45-N-8	479.2	390.59	0.18	303.6	0.37	236.68	0.51	423.03	0.12
Average value		/	/	0.16	/	0.27	/	0.59	/	0.19
Standard deviation		/	/	0.02	/	0.09	/	0.09	/	0.11

EV = experimental value; CV = calculated value; RE = relative error. *Based on consideration of the tensile strength of UHPC.

normal concrete, multilayer bridged by interlaminar fibers failure mode appeared in compression zone of the CA-UPHC slabs due to the fibers bridging effect.

(2) Postcracking ductility of the CA-UHPC slabs increases with the increment of reinforcement ratio obviously and gradually decreases with the expansion of cracks. The proposed new ductility index μ_{cr} increases from 2.83 to 74.97 when the reinforcement ratio rises from 0% to 3.45%, which excellently reflects the effects of reinforcement ratio on deflection ductility. In addition, a long ductile plateau stage in load-deflection curve is detected for specimens with high reinforcement ratio.

(3) Longitudinal reinforcement ratio presents greatly influences on stiffness of the specimens, which effectively delays the stiffness degradation of the specimens. For the reinforced slabs, nearly 50% of the initial stiffness remains when the longitudinal reinforcements yield. Thus, reinforcement with high strength and long yield platform will be an appropriate choice for the CA-UHPC structures.

(4) Flexural strength increases approximately linearly with the increment of longitudinal reinforcement ratio, while maximum aggregate size and curing method have no significant influence on structural behavior of the innovative CA-UHPC slabs, which greatly saves the budget and broadens the application field of CA-UHPC.

(5) The Chinese Code (CECS 38-2004), American Code (ACI 544.4R), British Standard (BS EN 1992) and modified British Standard (considering concrete tensile) are generally conservative in predicting the flexural capacity of the reinforced CA-UHPC slabs, with an average relative error of 0.16, 0.27, 0.59, and 0.19 relatively.

Data Availability

The experimental data used to support the findings of this study are included within the article.

Conflicts of Interest

The authors declare that they have no conflicts of interest.

Acknowledgments

The authors would like to thank the group members Fan Zhang, Kaiwei Lu, Wenchao Li, Kai Zhou, Qi Wang, Junzheng Zhu, and Changqing Chu for their contributions on the experimental works. This research was supported by the National Natural Science Foundation of China (Grant No. 51438003) and the Nanjing Public Engineering Project Construction Center (Grant No. 8505001327). It is also a project funded by the Priority Academic Program Development of Jiangsu Higher Education Institutions (PAPD, Grant No. CE02-1-10). The financial supports are greatly appreciated.

References

[1] F. Toutlemonde, J. Resplendino, L. Sorelli et al., "Innovative design of ultra high-performance fiber reinforced concrete ribbed slab: experimental validation and preliminary detailed analyses," in *Proceedings of the 7th International Symposium on Utilization of High Strength/High Performance Concrete*, pp. 1187–1206, Washington, DC, USA, June 2005.

[2] H. G. Russell, B. A. Graybeal, and H. G. Russell, "Ultra-high performance concrete: a state-of-the-art report for the bridge community," Report No. FHWA-HRT-13-060, Federal Highway Administration, Washington, DC, USA, 2013.

[3] J. Qi, Z. Wu, Z. J. Ma, and J. Wang, "Pullout behavior of straight and hooked-end steel fibers in UHPC matrix with various embedded angles," *Construction and Building Materials*, vol. 191, pp. 764–774, 2018.

[4] J. Liu, F. Han, G. Cui et al., "Combined effect of coarse aggregate and fiber on tensile behavior of ultra-high performance concrete," *Construction and Building Materials*, vol. 121, pp. 310–318, 2016.

[5] B. Graybeal, "Material property characterization of ultra-high performance concrete," Report No. FHWA-HRT-06-103, Federal Highway Administration, Washington, DC, USA, 2006.

[6] N. T. Tran, T. K. Tran, and D. J. Kim, "High rate response of ultra-high-performance fiber-reinforced concretes under direct tension," *Cement and Concrete Research*, vol. 69, pp. 72–87, 2015.

[7] J. Qi, Z. J. Ma, and J. Wang, "Shear strength of UHPC beams: mesoscale fiber-matrix discrete model," *Journal of Structural Engineering*, vol. 143, no. 4, article 04016209, 2016.

[8] J. Wang, J. Qi, T. Tong, Q. Xu, and H. Xiu, "Static behavior of large stud shear connectors in steel-UHPC composite structures," *Engineering Structures*, vol. 178, pp. 534–542, 2019.

[9] X. Shao, D. Yi, Z. Huang et al., "Basic performance of the composite deck system composed of orthotropic steel deck and ultrathin RPC layer," *Journal of Bridge Engineering*, vol. 18, no. 5, pp. 417–428, 2011.

[10] F. Lachance, J. P. Charron, and B. Massicotte, "Development of precast bridge slabs in high-performance fiber-reinforced concrete and ultra-high-performance fiber-reinforced concrete," *ACI Structural Journal*, vol. 113, no. 5, pp. 929–939, 2016.

[11] S. L. Yang, S. G. Millard, M. N. Soutsos, S. J. Barnett, and T. T. Le, "Influence of aggregate and curing regime on the mechanical properties of ultra-high performance fibre reinforced concrete (UHPFRC)," *Construction and Building Materials*, vol. 23, no. 6, pp. 2291–2298, 2009.

[12] M. Schmidt and E. Fehling, "Ultra-high-performance concrete: research, development and application in Europe," *ACI Special Publication*, vol. 228, pp. 51–78, 2005.

[13] J.-N. Qi, Z. J. Ma, J.-Q. Wang, and T.-X. Liu, "Post-cracking shear strength and deformability of HSS-UHPFRC beams," *Structural Concrete*, vol. 17, no. 6, pp. 1033–1046, 2016.

[14] S. Ghasemi, P. Zohrevand, A. Mirmiran, Y. Xiao, and K. Mackie, "A super lightweight UHPC-HSS deck panel for movable bridges," *Engineering Structures*, vol. 113, pp. 186–193, 2016.

[15] M. A. Saleem, A. Mirmiran, J. Xia et al., "Ultra-high-performance concrete bridge deck reinforced with high-strength steel," *ACI Structural Journal*, vol. 108, no. 5, pp. 601–609, 2011.

[16] M. A. Saleem, A. Mirmiran, J. Xia et al., "Experimental characterization of ultrahigh-performance concrete bridge deck system," *Journal of Bridge Engineering*, vol. 20, no. 9, article 04014101, 2014.

[17] M. S. Sumpter, S. H. Rizkalla, and P. Zia, "Behavior of high-performance steel as shear reinforcement for concrete beams," *ACI Structural Journal*, vol. 106, no. 2, pp. 122–124, 2010.

[18] A. Munikrishna, A. Hosny, S. Rizkalla et al., "Behavior of concrete beams reinforced with ASTM A1035 grade 100 stirrups under shear," *ACI Structural Journal*, vol. 108, no. 1, pp. 34–41, 2011.

[19] I. H. Yang, C. Joh, and B.-S. Kim, "Structural behavior of ultra high performance concrete beams subjected to bending," *Engineering Structures*, vol. 32, no. 11, pp. 3478–3487, 2010.

[20] M. M. Kamal, M. A. Safan, Z. A. Etman, and R. A. Salama, "Behavior and strength of beams cast with ultra high strength concrete containing different types of fibers," *HBRC Journal*, vol. 10, no. 1, pp. 55–63, 2014.

[21] C. Kahanji, F. Ali, and A. Nadjai, "Structural performance of ultra-high-performance fiber-reinforced concrete beams," *Structural Concrete*, vol. 18, no. 2, pp. 249–258, 2017.

[22] D.-Y. Yoo, N. Banthia, and Y.-S. Yoon, "Experimental and numerical study on flexural behavior of ultra-high-performance fiber-reinforced concrete beams with low reinforcement ratios," *Canadian Journal of Civil Engineering*, vol. 44, no. 1, pp. 18–28, 2017.

[23] U. Hasgul, K. Turker, T. Birol et al., "Flexural behavior of ultra-high-performance fiber reinforced concrete beams with low and high reinforcement ratios," *Structural Concrete*, vol. 19, no. 6, pp. 1577–1590, 2018.

[24] A. N. Dancygier and Z. Savir, "Flexural behavior of HSFRC with low reinforcement ratios," *Engineering Structures*, vol. 28, no. 11, pp. 1503–1512, 2006.

[25] W. I. Khalil and Y. R. Tayfur, "Flexural strength of fibrous ultra high performance reinforced concrete beams," *ARPN Journal of Engineering and Applied Sciences*, vol. 8, no. 3, pp. 200–214, 2013.

[26] J. Ma, M. Orgass, F. Dehn et al., "Comparative investigations on ultra-high performance concrete with and without coarse aggregates," in *Proceedings of the International Symposium on Ultra High Performance Concrete*, pp. 205–212, Kassel, Germany, September 2004.

[27] R. Ma, L. Guo, W. Sun, J. Liu, and J. Zong, "Strength-enhanced ecological ultra-high performance fibre-reinforced cementitious composites with nano-silica," *Materials and Structures*, vol. 50, no. 2, p. 166, 2017.

[28] Y.-W. Chan and S.-H. Chu, "Effect of silica fume on steel fiber bond characteristics in reactive powder concrete," *Cement and Concrete Research*, vol. 34, no. 7, pp. 1167–1172, 2004.

[29] K. Wille, A. E. Naaman, S. El-Tawil, and G. J. Parra-Montesinos, "Ultra-high performance concrete and fiber reinforced concrete: achieving strength and ductility without heat curing," *Materials and structures*, vol. 45, no. 3, pp. 309–324, 2012.

[30] Z. Wu, C. Shi, and W. He, "Comparative study on flexural properties of ultra-high performance concrete with supplementary cementitious materials under different curing regimes," *Construction and Building Materials*, vol. 136, pp. 307–313, 2017.

[31] L. F. A. Bernardo and S. M. R. Lopes, "Neutral axis depth versus flexural ductility in high-strength concrete beams," *Journal of Structural Engineering*, vol. 130, no. 3, pp. 452–459, 2004.

[32] R. Park, "Evaluation of ductility of structures and structural assemblages from laboratory testing," *Bulletin of the New Zealand National Society for Earthquake Engineering*, vol. 22, no. 3, pp. 155–166, 1989.

[33] J. Qi, J. Wang, and Z. J. Ma, "Flexural response of high-strength steel-ultra-high-performance fiber reinforced concrete beams based on a mesoscale constitutive model: experiment and theory," *Structural Concrete*, vol. 19, no. 3, pp. 719–734, 2018b.

[34] D.-Y. Yoo and Y.-S. Yoon, "Structural performance of ultra-high-performance concrete beams with different steel fibers," *Engineering Structures*, vol. 102, pp. 409–423, 2015.

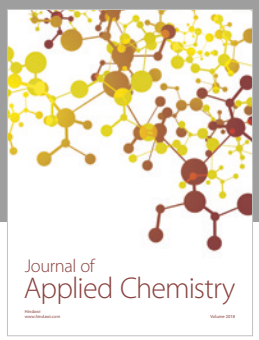

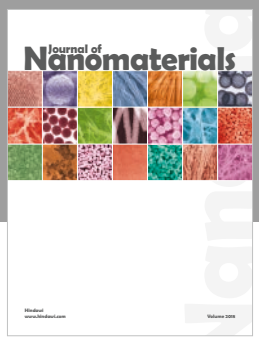

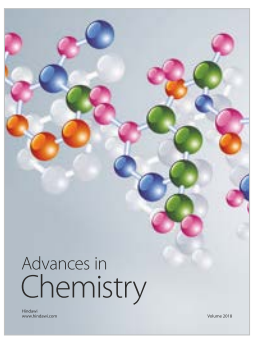

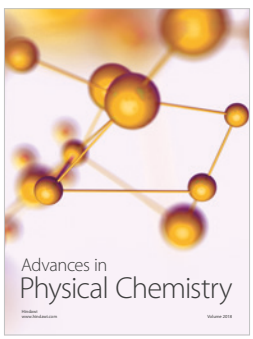

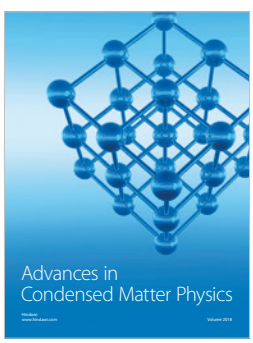

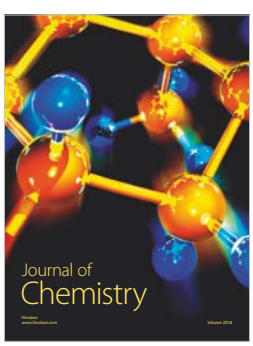

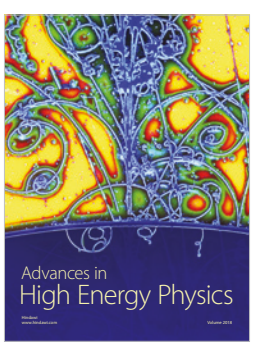

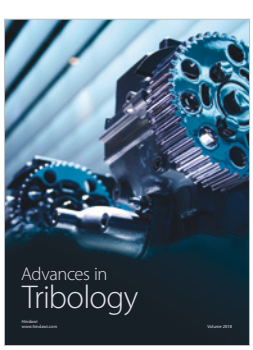

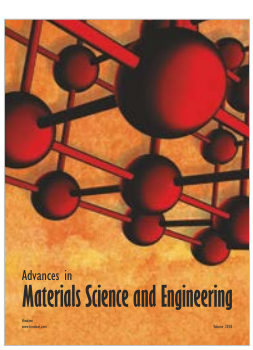

Hindawi

Submit your manuscripts at
www.hindawi.com